The priming phosphorylation of KaiC is activated by the release of its autokinase autoinhibition

Yoshihiko Furuike[a,b], Yasuhiro Onoue[a], Shinji Saito[b,c], Toshifumi Mori[d,e,*], Shuji Akiyama[a,b,*]

[a]Research Center of Integrative Molecular Systems (CIMoS), Institute for Molecular Science, National Institute of Natural Sciences, 38 Nishigo-Naka, Myodaiji, Okazaki 444-8585, Japan.

[b]Molecular Science Program, Graduate Institute for Advanced Studies, SOKENDAI, 38 Nishigo-Naka, Myodaiji, Okazaki 444-8585, Japan.

[c]Department of Theoretical and Computational Molecular Science, Institute for Molecular Science, National Institute of Natural Sciences, 38 Nishigo-Naka, Myodaiji, Okazaki 444-8585, Japan.

[d]Institute for Materials Chemistry and Engineering and Interdisciplinary, Kyushu University, Kasuga, Fukuoka 816-8580, Japan.

[e]Graduate School of Engineering Sciences, Kyushu University, Kasuga, Fukuoka 816-8580, Japan.

*Toshifumi Mori and *Shuji Akiyama

Email: toshi_mori@cm.kyushu-u.ac.jp (T.M.), akiyamas@ims.ac.jp (S.A.)

Author Contributions: Y.F., T.M., and S.A. designed the research. Y.F. and Y.O. conducted biochemical experiments. Y.F. and S.A. analyzed structural data. T.M. and S.S. performed simulations. S.A., Y.F., and T.M. wrote the paper with input from all authors.

Competing Interest Statement: The authors declare no competing interests.

Classification: Biological Sciences; Biochemistry.

Keywords: Circadian Clock | Cyanobacteria | KaiC | Kinase | Priming Phosphorylation

This PDF file includes:

Main Text
Figures 1 to 6

Abstract

KaiC, a cyanobacterial circadian clock protein with autokinase activity, catalyzes the dual phosphorylation of its own S431 and T432 residues in a circadian manner in the presence of KaiA and KaiB. Priming phosphorylation at T432 is a key step that promotes secondary phosphorylation at S431. Although KaiA binding is considered essential for KaiC phosphorylation, the mechanisms underlying the activation and inactivation of priming phosphorylation remain elusive. We found that

the priming phosphorylation proceeds even in the absence of KaiA, but is autoinhibited within KaiC, which decreases the rate constant to 0.019 h^{-1}. The autoinhibition of KaiC and the mechanism underlying the release from autoinhibition by KaiA were examined by KaiC structural analysis, and by classical molecular dynamics and quantum mechanics / molecular mechanics simulations. We found that the side chain of T432 adopts two rotamers in dephosphorylated KaiC, one of which places T432 in a position suitable for a nucleophilic attack on the terminal phosphate of adenosine triphosphate (ATP). However, the nucleophilicity of T432 was insufficient to overcome an energy barrier of approximately 22 kcal mol^{-1} because the catalytic function of a nearby base, E318, was self-suppressed by hydrogen bonding to positively charged R385. Biochemical assays of KaiC mutants showed that the autoinhibition of KaiC autokinase activity is attenuated by conferring T432 high nucleophilicity through the KaiA-assisted release of R385 from E318 to E352. During the circadian cycle, R385 switches interacting partners to inactivate/activate the autokinase function and to ensure the unidirectionality of the KaiC phosphorylation cycle.

Significance Statement

KaiC, a central player in the circadian clock system of cyanobacteria, undergoes an ordered phosphorylation cycle in the presence of KaiA and KaiB. To elucidate the mechanism underlying the rhythmic regulation of the KaiC autokinase, we performed structural analyses, computational simulations, and biochemical assays of KaiC and its mutants. The results indicate that KaiC is essentially an autoinhibited autokinase, and the autoinhibition of primary phosphorylation at its T432 residue is attenuated by conferring it high nucleophilicity against the terminal phosphate of adenosine triphosphate. KaiA contributes to releasing the autoinhibition of KaiC in a morning phase by switching the interacting partners of R385 from a catalytic glutamate E318 to E352, as well as ensuring unidirectionality of the KaiC phosphorylation cycle.

Main Text

Introduction

Circadian clocks are time-keeping systems that enable organisms to adapt to daily changes in environmental conditions by modifying intracellular processes. The clock systems from bacteria to mammals share three physiological characteristics (1): self-sustained oscillation with an approximately 24 h period, an endogenous period of temperature insensitivity (temperature compensation), and a phase entrainment in response to external stimuli. These properties depends on complex and diverse biochemical events involving clock proteins and clock-related components (2, 3).

Phosphoryl modification is one of the main post-translational events regulating clock proteins. Phosphorylation of the clock proteins modulates their function, atomic-scale structure, and dynamics, thereby controlling the stoichiometry and stability of multimeric clock-protein complexes (4, 5). Rhythmic phosphorylation of the clock proteins is observed in many organisms (6, 7) as well as *in vitro* reconstituted systems (8, 9). To achieve a circadian rhythm of phosphorylation, at least two processes for activating and inhibiting phosphorylation must be present, and these processes must switch appropriately from phase to phase.

Protein kinases phosphorylate targeted amino acids such as Ser, Thr, and Tyr in a substrate molecule or in the kinase itself (autokinase). Kinases can be constitutively active or switch between the active and inactive forms through intermolecular interactions or autophosphorylation (10). The activity of constitutively activate kinases with external substrates can be modulated by the concentration of the substrate. However, the activity of autokinases is controlled by modifying the active site structure or the intramolecular accessibility to the targeted amino acids.

KaiC is a component of the cyanobacterial circadian clock of *Synechococcus elongatus* PCC 7942 that possesses autokinase activity. KaiC is composed of tandemly duplicated N-terminal (CI) and C-terminal (CII) domains (11), and it forms a double-ring hexamer by incorporating one molecule of ATP or ADP at every CI–CI and CII–CII interface (12). In the presence of KaiA and KaiB, the S431 and T432 residues in the CII domain of KaiC are phosphorylated/dephosphorylated

in a circadian manner (13). The protein undergoes a phosphorylation cycle starting in a fully dephosphorylated form (KaiC-ST) and changing to a T432-phosphorylated form (KaiC-SpT: priming phosphorylation), a S431/T432-phosphorylated form (KaiC-pSpT: secondary phosphorylation), and a S431-phosphorylated form (KaiC-pST) before returning to the KaiC-ST form (14, 15). Studies indicate that the phosphoryl modification of KaiC-ST proceeds only after the addition of KaiA (13). KaiA does not show amino acid sequence or structure similarity with other existing kinases, suggesting that binding of KaiA to KaiC is necessary for the autophosphorylation of KaiC. Although the function and structure of the KaiA–KaiC complex have been studied extensively (16-18), the dynamic nature of the KaiA–KaiC complex has made these studies difficult, and the mechanism underlying the regulation of KaiC autokinase activity remains to be elucidated.

In the absence of KaiA, KaiC is present in the KaiC-ST form under physiological conditions (19-21); therefore, the priming phosphorylation of T432 is frequently discussed in relation to the KaiA binding (13, 18). However, in this study we found that KaiC is autophosphorylated in the absence of KaiA, albeit at a slower rate. Although this finding is not consistent with the conventional interpretation that KaiC cannot be auto-phosphorylated in the absence of KaiA, it suggests that the priming phosphorylation of KaiC is activated by releasing the autoinhibition of autophosphorylation activity through interaction with KaiA. This finding provides an opportunity to examine the mechanism by which KaiA activates KaiC autophosphorylation by analyzing the autoinhibition of KaiC without using KaiA.

In this study, we revisited our previous crystal structure of KaiC-ST to examine the mechanism underlying the autoinhibition of KaiC autophosphorylation. The priming phosphorylation of KaiC at T432 was examined using classical molecular dynamics (MD) and quantum mechanics/molecular mechanics (QM/MM) simulations, and the energy barrier for the phosphoryl transfer reaction mediated by the identified catalytic base was estimated. Amino acid substitutions in the catalytic base and regulatory residues nearby suggest a mechanism by which the KaiC autophosphorylation is autoinhibited, and this inhibition is released by interaction with KaiA.

Results

Priming Phosphorylation at T432 in KaiC Occurs Even in the Absence of KaiA, Albeit at a Slower Rate. At a standard experimental temperature of 30°C (19-21), KaiC underwent the auto-dephosphorylation and was eventually detected in a fully dephosphorylated from, KaiC-ST (Fig. 1*A* and *SI Appendix*, Fig. S1). After 40 h of incubation at 30°C, a small fraction of KaiC remained in the KaiC-SpT, KaiC-pSpT, and KaiC-pST forms, which did not change detectably after another 20 h.

Next, we performed a densitometric analysis of the gel image (Fig. 1*A*) and carefully examined the resultant kinetic traces for autodephosphorylation (Fig. 1*B*). Consistent with previous reports (19-21), the KaiC-SpT and KaiC-pSpT fractions decreased rapidly, whereas the KaiC-pST fraction increased transiently and then began to decrease, and the KaiC-ST form increased progressively. At 40–60 h of incubation, the fractions of KaiC-SpT, KaiC-pSpT, and KaiC-pST remained constant at approximately 0.03, 0.02, and 0.06, respectively (Fig. 1*B*, Inset). KaiA was previously reported to be essential for the autophosphorylation of KaiC-ST at 30°C (13). However, the present observations imply that KaiC-ST is autophosphorylated even in the absence of KaiA, albeit at a slower rate.

As shown by solid lines in Fig. 1*B*, the global-fitting of a reversible four-state cyclic model (14, 15) was used to examine the autodephosphorylation dynamics of KaiC, and the eight associated rate constants were determined (Fig. 1*C*).The contributions of the priming (KaiC-ST → KaiC-SpT, $k_1 = 1.9 \pm 0.3 \times 10^{-2}$ h^{-1}) and secondary (KaiC-SpT → KaiC-pSpT, $k_2 = 1.7 \pm 0.4 \times 10^{-1}$ h^{-1}) autophosphorylation events were considerable and reproducible (n = 5, *SI Appendix*, Table S1), even when the reaction was initiated using different relative amounts of KaiC in the four states (*SI Appendix*, Fig. S2). When both k_1 and k_2 were forced to zero while keeping the others unchanged, the fitting to the residual phosphorylated species became considerably poorer, supporting this model (Fig. 1*B*, dashed lines). To confirm this interpretation, we showed that KaiC,

which was dephosphorylated by equilibration at pH 8 for 50 h at 30°C, was slightly but obviously phosphorylated after the pH was increased to 9.0 (Fig. 1*D* and *SI Appendix*, Fig. S3).

The present data and analysis suggest that the priming phosphorylation of KaiC-ST occurs slowly but continuously in the absence of KaiA, even under steady-state conditions in which KaiC-ST is the predominant form over other phosphorylated forms at 30°C (Fig. 1*B*). As illustrated in the model in Fig. 1*C*, approximately 60% [k_{-1} / (k_{-1} + k_2)] of the minor KaiC-SpT form is directly converted back to KaiC-ST; however, the remaining 40% undergoes secondary auto-phosphorylation and is restored to the KaiC-ST form by autodephosphorylation in a cyclic manner. At 30°C, a small amount of KaiC-SpT, the product of the priming phosphorylation, undergoes a repeated cycle of formation and loss even in the absence of KaiA.

One of Two Rotamers of T432 in KaiC-ST is Near Ready for the Autokinase Substrate. The molecular mechanism of the priming phosphorylation remains under debate partly due to the limited spatial resolution of the KaiA–KaiC complex (16-18). The slow but steady priming phosphorylation of KaiC in the absence of KaiA suggests that the structure of KaiC-ST itself could be used to examine this mechanism.

We thus inspected the existing crystal structure of KaiC-ST (22) from the perspective of priming phosphorylation. An ATP molecule bound between two neighboring CII protomers (CII-ATP, Fig. 2*A*) serves as the phosphate source for the kinase reaction. S431, T432, and a phospho-switch (PSw) belonging to one protomer, together with E318*, E352*, and R385* belonging to a second protomer (hereafter, marked with asterisks), constitute an active site around CII-ATP (Fig. 2*B*). The PSw located at the upstream of S431 undergoes a helix-coil transition according to the phosphoryl modification essentially at S431 (22). In KaiC-ST, the helical conformation of the PSw facilitates positioning of T432 closer to CII-ATP than S431 (Fig. 2*B*), which is favorable for the priming phosphorylation reaction (22).

The side chain of T432 adopted two conformations corresponding to a rotation of 120° around the C_α – C_β axis. Refinement using only one rotamer (rotamer A), in which the T432 O_γ was oriented toward the phosphorus atom (P_γ) of the γ-phosphate group of CII-ATP, yielded a small but obvious positive difference Fourier peak near T432 C_β (magenta arrow in Fig. 2*C*). Refinement using the other rotamer (rotamer B) showed a similar but separate peak with the T432 O_γ directed away from CII-ATP (Fig. 2*D*). The occupancy of each rotamer was estimated at approximately 50% (Fig. 2*E*).

T432 O_γ of rotamer A ($T432^{rot\text{-}A}$ O_γ) was nearly configured as a suitable substrate for kinase reactions. In general, Thr or Ser reacts with an ATP molecule through an S_N2-like transition structure (Fig. 2*F*), in which the nucleophilic O_γ is brought as close as possible to the ATP P_γ along with the ATP P_γ – $O_{3\beta}$ axis to form an O_γ – ATP P_γ bond, and the ATP P_γ – $O_{3\beta}$ bond is then cleaved in a concerted manner. $T432^{rot\text{-}A}$ O_γ was only 4.1 Å away from the ATP P_γ with a $T432^{rot\text{-}A}$ O_γ –CII-ATP P_γ – CII-ATP $O_{3\beta}$ angle of 158° (Fig. 2*F*), which is an almost optimal in-line position (~3 Å and 180°) for the reaction. $T432^{rot\text{-}B}$ O_γ was in a less favorable position (5.8 Å and 141°) than $T432^{rot\text{-}A}$ O_γ.

To become a ready-to-react nucleophile, the hydroxyl group of $T432^{rot\text{-}A}$ has to be deprotonated by a common base. In KaiC-ST, $T432^{rot\text{-}A}$ O_γ could potentially be hydrogen-bonded to E318* O_ε with a distance of 3.6 Å (Fig. 2*C*). In fact, the E318Q substitution inhibited the priming phosphorylation in the presence of KaiA (Fig. 2*G*), suggesting that E318* O_ε attracts $T432^{rot\text{-}A}$ H_γ through a hydrogen-bonding interaction, and $T432^{rot\text{-}A}$ O_γ becomes the reactive nucleophile. These structural analyses suggest that the rotamer A is the structural basis for the slow but steady priming phosphorylation of KaiC-ST.

QM/MM and MD Simulations of a Proton Transfer and T432 Phosphorylation Reaction. To visualize the priming phosphorylation independent of KaiA, we performed QM/MM metadynamics (metaD) simulation using the KaiC-ST hexamer with $T432^{rot\text{-}A}$ as the initial coordinate. In the simulations, we used a QM region consisting of the side chains of $T432^{rot\text{-}A}$, E318*, R385*, and part of CII-ATP/Mg^{2+} (Fig. 3*A*, represented by green or orange stick models).

The QM/MM metaD suggested that T432$^{rot\text{-}A}$ O_γ is activated as a nucleophile and attacks CII-ATP P_γ in synergy with E318*. As shown in Fig. 3*B*, E318* O_ε attracted the configured T432$^{rot\text{-}A}$ H_γ through a hydrogen-bonding interaction prior to dissociating the γ-phosphate from CII-ATP, thereby directing the hydroxyl of T432$^{rot\text{-}A}$ to the ready-to-react orientation (reactant in Fig. 3*B*). The obtained trajectory shows that the CII-ATP P_γ – CII-ATP $O_{3\beta}$ bond dissociated to form an intermediate state at 160 ps. After remaining in the intermediate state, the system moved to a transition state by decreasing the T432$^{rot\text{-}A}$ O_γ – E318* O_ε distance to ~3 Å; at this moment, a covalent bond was formed between P_γ and T432$^{rot\text{-}A}$ O_γ concomitant with the transfer of T432$^{rot\text{-}A}$ H_γ to E318* (product in Fig. 3*B*). This suggests that both the formation of the P_γ – T432$^{rot\text{-}A}$ O_γ bond and the proton transfer from T432$^{rot\text{-}A}$ O_γ to E318* O_ε need to be considered to describe the transition state of the phosphoryl transfer step.

To identify possible reaction pathways, we calculated the two-dimensional free energy surface as a function of the relative positions of CII-ATP P_γ and T432$^{rot\text{-}A}$ H_γ. As the reaction proceeded from the intermediate state (lower left in Fig. 3*C*), the CII-ATP P_γ – T432$^{rot\text{-}A}$ O_γ distance (r_1) became shorter, whereas the CII-ATP P_γ – CII-ATP P_β distance (r_2) increased ($r_2 - r_1 = q_1$ increased). After the q_1 value reached 2.5, the attraction of T432$^{rot\text{-}A}$ H_γ by E318* O_ε shortened the T432$^{rot\text{-}A}$ H_γ – E318* O_ε distance (r_3) but lengthened the T432$^{rot\text{-}A}$ H_γ – T432$^{rot\text{-}A}$ O_γ distance (r_4) ($r_4 - r_3 = q_2$ increased). The most plausible reaction pathways emerged as diagonal clefts from the lower left to the upper right corners in Fig. 3*C*. Together with the one-dimensional free energy surface connecting the reactant and intermediate states (Fig. 3*D*), the present simulations suggest a barrier as high as approximately 22 kcal mol^{-1} to yield KaiC-SpT from KaiC-ST.

In a separate MD simulation, the side chain of T432 in five of the six protomers of KaiC-ST was re-oriented to fit the rotamer B during the simulation, whereas one survived as rotamer A for 1 μs mostly within approximately 5 Å from CII-ATP P_γ (*SI Appendix*, Fig. S4). This implies that the ready-to-react structures with the short T432$^{rot\text{-}A}$ O_γ – CII-ATP P_γ distance exist in solution in a short-lived state, i.e., a conformationally excited state (23). The high energy barrier and the limited population of ready-to-react structures suggest that the priming phosphorylation of T432 in KaiC-ST is not efficient in the absence of KaiA. This is consistent with experimental observations that only a small amount of pT432 is produced from KaiC-ST at 30°C (Fig. 1*A* and 1*B*). The accumulation of KaiC-SpT in the presence of KaiA (Fig. 2*G*) suggests that KaiA plays a role in lowering the energy barrier by enhancing the nucleophilic character of T432$^{rot\text{-}A}$ O_γ.

R385* Indirectly Regulates the Nucleophilicity of T432$^{rot\text{-}A}$ O_γ for Priming Phosphorylation. The nucleophilicity of T432$^{rot\text{-}A}$ O_γ can be enhanced by strongly withdrawing its proton, T432$^{rot\text{-}A}$ H_γ. Although the negatively charged carboxylate moiety of E318* appears to be in an ideal position for this purpose, its negative charge is partially neutralized by hydrogen bonding with the positively charged guanidino moiety of R385* (Fig. 2*B*).

We tested the indirect effects of R385* on the nucleophilicity of T432$^{rot\text{-}A}$ O_γ using a KaiC^{R385A} mutant (24). The R385A substitution dramatically accelerated the priming phosphorylation of T432, resulting in the conversion of KaiC^{R385A}-ST to KaiC^{R385A}-SpT and then to KaiC^{R385A}-pSpT regardless of the presence of KaiA (Fig. 4*B* and 4*C*). This result indicates that R385* hydrogen-bonded to E318* neutralizes the negative charge of E318* and indirectly suppresses the nucleophilicity of T432$^{rot\text{-}A}$ O_γ. To determine the range of the indirect effects on T432$^{rot\text{-}A}$ O_γ, we examined the hydrogen-bonding network in KaiC-ST from T432$^{rot\text{-}A}$ O_γ to E318*, R385*, and even E352* (Fig. 2*B*). A KaiC^{E352Q} mutant in which the charge at the 352nd position was neutralized showed a markedly reduced rate of decrease in the ST state in the presence of KaiA (Fig. 4*D*) compared with wild-type KaiC (Fig. 4*A*). Similar observations were made for a KaiC^{E352D} mutant (Fig. 4*E*) in which the side chain at the 352nd position remained negatively charged, but not long enough to form a hydrogen bond with R385*. One possible reason for the observed deceleration of the primary phosphorylation is the destabilization of the KaiA-induced state with R385* sequestered in the direction of the 352nd position. These results suggest that in KaiC-ST, R385* neutralizes the negative charge of E318*, eventually suppressing the nucleophilicity of T432$^{rot\text{-}A}$ O_γ, whereas E352* tends to antagonize the effect of R385*.

The above interpretation is also supported by the crystal structure of a S431A/T432A mutant (KaiC-AA) that mimics KaiC-ST bound by KaiA (25). The side chain of R385*, which interacted with E318* at a distance of 3.3 Å in KaiC-ST (Fig. 5*A*), was separated from E318* by a distance of 5.2 Å (Fig. 5*B*). The present biochemical and structural data imply that the effective priming phosphorylation of T432 is achieved by conferring $T432^{rot\text{-}A}$ O_γ high nucleophilicity through a KaiA-assisted conformational change that results in the attraction of R385* to E352* via the hydrogen bonds and liberates R385* from E318*.

R385* Rearrangement Assures the Unidirectionality of the KaiC Phosphorylation Cycle. The existing library of the KaiC structures (22, 25) suggests the crucial role of R385* rearrangement even after priming phosphorylation. In the T432E mutant (KaiC-SE), which is considered the most accurate KaiC-SpT mimetic (14, 26), R385* is pulled away from E318* by hydrogen bonds with E432 and E352* (Fig. 5*C*), leaving E318* activated as the reactive base suitable for attracting a hydrogen atom. This orientation of R385* in KaiC-SE may be effective in promoting the E318*-mediated activation of S431 O_γ for the secondary phosphorylation reaction.

In nine of the fifteen pSpT protomers in the library (Fig. 5*D*, right), the positively charged guanidino moiety of R385* was trapped by the negatively charged side chain of D417*. Although R385* in the other six protomers remained within the interaction range of E352*, the distance between R385* and E318* was considerably longer than the hydrogen bonding distance (Fig. 5*D*, left). These findings suggest that E318* of KaiC-pSpT remains as the active free base, despite the lack of reactive side chains for the kinase reaction around CII-ATP. In such an arrangement of R385*, however, KaiC-pST could be autophosphorylated again and re-converted to KaiC-pSpT. In seven of the ten pST protomers in the library, the side chain of T432 in KaiC-pST, which may restrain this reverse reaction, formed a third rotamer C (Fig. 5*E*) with its hydroxyl group oriented away from E318* and trapped by R385* (Fig. 5*E*, left).

The coil-to-helix transition of PSw (22), which is promoted by the autodephosphorylation of pS431, returns R385* to the configuration observed in KaiC-ST (Fig. 5*A*). During the circadian cycle, the positively charged guanidino group of R385* swaps interacting partners among E318*, E352*, and D417* to achieve inactivation/activation of $T432^{rot\text{-}A}$ O_γ, thereby ensuring the unidirectionality of the phosphorylation cycle of KaiC.

Discussion

Although KaiA is considered essential for the phosphorylation of KaiC (13), the present findings clearly demonstrate that the priming phosphorylation of T432 occurs at 30°C in the absence of KaiA, albeit at a slower rate. Even under conditions that promote the steady-state predominance of KaiC-ST, <10% of KaiC is transiently expressed as partly or fully phosphorylated forms and constantly cycling among the four states (Fig. 1*C*). The low abundance of these forms is mainly due to inefficient priming phosphorylation, which is limited by the three factors described below.

The first is the marginal stability of the helical PSw in KaiC-ST in solution. The structure of the PSw changed from a helical to a non-helical form in five of six protomers in the QM/MM simulation over a period of 1 μs. This observation is also consistent with our recent mutation study (27), which identified structural polymorphisms of the PSw in KaiC-ST mimetics. The helix-to-coil transition of the PSw causes the hydroxyl group of T432 to face the opposite direction to CII-ATP (Fig. 5*E*), and the resultant location of T432 downstream of the coiled PSw is unfavorable for the kinase reaction.

The second limiting factor is the rotamers of T432 located downstream of the helical PSw. In KaiC-ST carrying the helical PSw, the side chain of T432 shuttles between the two rotamers A and B, waiting for a chance to attack CII-ATP P_γ. Considering that one half of the rotamers in one-sixth of the KaiC-ST protomers are enabled to react, the fraction of T432 that can undergo the kinase reaction is estimated to be approximately 10%.

This ~10% of the population is limited by the third factor, an energy barrier that can be as high as 22 kcal mol^{-1}. The barrier-crossing mechanism can be largely categorized into base-assisted and substrate-assisted mechanisms (28), which differ in the pathway for withdrawing a proton from the hydroxyl group of Ser or Thr. In the base-assisted mechanism, the substrate proton

is transferred to a basic residue nearby, for example from T432$^{rot\text{-}A}$ O_γ to E318* O_ε in KaiC-ST in the absence of KaiA (Fig .3*B*). By contrast, in the substrate-assisted mechanism, the substrate proton is directly transferred to one of the three oxygen atoms of the γ-phosphate. The following observations support that the priming phosphorylation occurs in a base-assisted manner: The lone pair of E318* is directly oriented toward T432$^{rot\text{-}A}$ O_γ, whereas CII-ATP O_γ closest to T432 is already involved in a hydrogen bond with T290* and an electrostatic interaction with K294* (*SI Appendix*, Fig. S5). The current QM/MM metaD simulation also found the hydrogen bond between E318* O_ε and T432$^{rot\text{-}A}$ H_γ prior to the dissociation of the CII-ATP P_γ – CII-ATP $O_{3\beta}$ bond (Fig. 3*B*), and the free energy surfaces further support this mechanism (Fig. 3*D*). Furthermore, the E318Q substitution suppressed the kinase activity in the presence of KaiA (Fig. 2*G*). These factors led us to conclude that the priming phosphorylation of KaiC-ST follows the base-assisted mechanism, regardless of the presence of KaiA.

It is important to discuss our observations with respect to previous QM/MM studies (see (29) and references are therein). QM/MM simulations have been used to investigate phosphoryl transfer reactions in several kinases, including cAMP-dependent protein kinase (30-34), cyclin-dependent kinase (35-37), and N-acetyl-L-glutamate kinase (38, 39). In these examples, the activation energy for the phosphoryl transfer reaction ranges from 10 to 25 kcal mol^{-1}. The present QM/MM simulation is the first example of the visualization of atomic-scale details before and after the phosphoryl transfer reaction in clock proteins. The reason for this is that high-resolution structures of fully dephosphorylated clock proteins were not available for a long time, as is the case for KaiC (22). The activation energy for T432$^{rot\text{-}A}$ in KaiC-ST, which is approximately 22 kcal mol^{-1}, is within the above range, suggesting that once formed, it can be phosphorylated on a reasonable time scale even in the absence of KaiA. According to the Eyring equation, the present experimental rate constant (k_1 = 1.9 ± 0.3 × 10^{-2} h^{-1}) for the priming phosphorylation of T432 without KaiA corresponds to an activation energy of 25 kcal mol^{-1}. The discrepancy may be due to the setup or the limited accuracy of our QM/MM calculations, although it may also mean that the contribution of the second factor is larger than the above estimate.

The present results suggest that the binding of KaiA attenuates at least one of the limiting factors for the priming phosphorylation of KaiC-ST. The structural and QM/MM evaluations clearly indicate that the carboxylate side chain of E318* attracts T432$^{rot\text{-}A}$ H_γ and enhances the nucleophilicity of T432$^{rot\text{-}A}$ O_γ (Fig. 3*B*). This function of E318* as the inherent base is, however, self-suppressed in KaiC-ST by the neutralization of its negative charge with the positively charged guanidino group of R385* nearby. As demonstrated using the KaiC^{R385A} (Fig. 4*B* and 4*C*) and KaiC-AA (Fig. 5*B*) mutants, binding of KaiA attenuates this self-suppression by sequestering R385* from E318* to E352*. The observed decay of the KaiC-ST form in the presence of KaiA (Fig. 4*A*) suggests that the rate constant of the priming phosphorylation reaction should increase by a factor of at least 15. This is equivalent to a reduction of the energy barrier of approximately 2 kcal mol^{-1} caused by enhancing the nucleophilicity of the substrate through the KaiA–KaiC interaction. The present results show that the priming auto-phosphorylation is self-suppressed, although not completely, in KaiC-ST, whereas that KaiA attenuates this self-suppression to achieve the KaiC autophosphorylation on a reasonable time scale as a circadian clock system.

Common protein kinases are maintained mostly inactive in the absence of activating upstream stimuli, whereas inhibitory factors are removed at the biologically appropriate times and locations. As reviewed in detail by Reinhardt and Leonard (10), there are many systems for maintaining protein kinases inactive, such as blocking ATP binding (40), sequestration of substrates or blocking their access (41-44), occupation or occlusion of catalytic cleft (45-47), and binding of regulatory proteins (48).

In most of these examples, positively charged side chains located within hydrogen-bonding distance to the catalytic glutamate/aspartate are extremely limited. Conserved downstream Lys residues that are intrinsically close to the catalytic aspartate (3.3-4.7 Å) are unlikely to form stable hydrogen bonds, regardless of their activation or inactivation, because the carboxylate plane of the catalytic aspartate is almost perpendicular to the orientation of the Lys (*SI Appendix*, Fig. S6*A*). This is also the case for casein kinase 1 delta (CK1d), which is essential for the pacemaker function of mammalian clock systems (49). Insulin receptor kinase (40) and the Src family of tyrosine

kinases (43) are exceptions because their catalytic glutamate forms a hydrogen bond with the Arg residue located two or four residues downstream; however, these kinases are not in the ATP-bound form (*SI Appendix*, Fig. S6*B*). This means that, in contrast to KaiC, most protein kinases switch between the active and inactive forms by regulating the substrate access and by autophosphorylating their activation loop (50-53); their catalytic glutamates thus remain unsuppressed to efficiently withdraw a proton from the substrate. KaiC encapsulates both a braking function to fulfill the circadian timescale through the interaction of R385* and E318* and an accelerating function to promote the priming phosphorylation in a morning phase through the interaction of R385* and E352*.

The priming phosphorylation in KaiC can be summarized as follows: The side chain of T432, which was sequestered as the rotamer C in KaiC-pST (Fig. 6*A*), shuttles between two rotamers, A and B, in KaiC-ST to optimize its attack of CII-ATP P_γ (Fig. 6*B*). The primary phosphorylation proceeds, albeit slowly, in the ST state even in the absence of KaiA, but its efficiency is low because the function of E318* as the catalytic base to enhance the nucleophilicity of T432 O_γ is autoinhibited by R385* (Fig. 6*C*). KaiA binds to the C-terminus of KaiC (16, 17) and releases this autoinhibition by switching the interacting partner of R385* from E318* to E352* (Fig. 6*D*). The increased nucleophilicity of E318* facilitates the attraction of $T432^{rot\text{-}A}$ H_γ, resulting in the concerted proton transfer from $T432^{rot\text{-}A}$ to E318* and the nucleophilic attack of CII-ATP P_γ by $T432^{rot\text{-}A}$ O_γ (Fig. 6*D*). In KaiC-SpT (Fig. 6*E*), R385* remains evacuated from E318* by the phosphorylated T432 to promote the secondary phosphorylation at S431.

Materials and Methods

Expression and Purification of KaiC and its Mutants. Glutathione S-transferase (GST)-tagged KaiC was constructed in the plasmid vector, pGEX-6P-1. GST-tagged KaiC was expressed in *E. coli.* BL21(DE3) and purified as previously reported (14). The purified KaiC was dissolved in a buffer containing 20 mM Tris-HCl (pH8), 150 mM NaCl, 1 mM ATP, 5 mM $MgCl_2$, 0.5 mM ethylenediaminetetraacetic acid (EDTA), and 1 mM dithiothreitol (DTT) (buffer A).

KaiC Auto-dephosphorylation Assay. WT-KaiC (0.6 mg/mL) was incubated at 30°C to induce autodephosphorylation. Aliquots were taken from the incubated samples at pseudo logarithmic intervals using the automated sampling device (54) to cover fast and slow relaxations quantitatively. The relative abundance of four phosphorylated KaiC forms was quantified by SDS polyacrylamide gel electrophoresis (SDS-PAGE) using LOUPE software (54). Kinetic traces for autodephosphorylation dynamics were fitted using a reversible four-state cyclic model as shown in Fig. 1*C* using MATLAB software.

KaiC Auto-phosphorylation Assay. WT-KaiC was pre-incubated in buffer A for 50 h at 30°C to induce autodephosphorylation. The pH of the sample solution was changed using a buffer consisting of 20 mM Tris-HCl (pH9), 150 mM NaCl, 1 mM ATP, 5 mM $MgCl_2$, 0.5 mM EDTA, and 1 mM DTT in a desalting column, PD MiniTrap G-25 (Cytiva). The sample solution at pH 9 (0.4 mg/mL) with abundant KaiC-ST was incubated at 30°C. Sampling and analyses were performed as described for the autodephosphorylation assay.

KaiA-assisted Phosphorylation Assay. WT-KaiC and the KaiC mutants $KaiC^{E352Q}$ and $KaiC^{E352D}$ were pre-incubated in buffer A for 48 h at 30°C to induce autodephosphorylation. The KaiC solutions (0.2 mg/mL) were then mixed with KaiA (0.04 mg/mL) and the phosphorylation status was analyzed by SDS-PAGE. For $KaiC^{R385A}$, the pre-incubation step was omitted and the sample solution was directly transferred to 30°C and mixed with KaiA.

Analysis of the Crystal Structure of KaiC. In this study, the seven coordinates (PDB code: 7DYJ, 7DYE, 7DYI, 7DY1, 7DY2, 7DXQ, and 7V3X) deposited in the PDB databank were used for the analysis. The graphical presentations were generated by using Pymol.

QM/MM and MD Simulations. The initial coordinates of the KaiC-ST hexamer with T432$^{rot\text{-}A}$ were obtained from PDB: 7DYJ, and the loops that were missing from the crystal structure were modeled according to the previously reported structure (PDB: 2GBL) (17). The flexible N- and C-termini of KaiC-ST were omitted, i.e., residues I18–I497 of each KaiC-ST monomer were used. In addition, 12 ATP molecules, 12 magnesium ions, and crystal water molecules within the protein molecules were included in the system. Hydrogen atoms were added using the LEAP module in AmberTools. The KaiC-ST hexamer was surrounded by a water layer of 11.0 Å thickness and placed in a rectangular box. Sodium ions were added to neutralize the system charge. The total number of atoms in the system was thus approximately 207,000.

The Amberff99SB-ILDN force field (55) was used for the protein molecules, with modified parameters for ATP (56). The TIP3P model (57) was used for the water molecules. Long-range electrostatic interactions were treated using the particle mesh Ewald method (58), whereas short-range non-bonded interactions were cut off at 10 Å. A time step of 2 fs was used, and the simulations were performed using the Amber 2018 software (59) and the PLUMED 2.5.3 package (60).

The energy of each system was minimized for 1,000 steps while allowing only hydrogens to relax, followed by energy minimizations of 10,000 steps with restraints on backbone atoms to relax the sidechains and 10,000 steps without restraints. The temperature of the system was then gradually increased to 300 K over 100 ps while restraining the backbone atoms with a weak force constant of 1.0 kcal mol^{-1}. Next, a constant-NPT (300 K, 1 atm) simulation was performed for 500 ps under the same restraint, followed by another 500 ps of constant-NPT (300 K, 1 atm) simulation without restraints. Finally, a 10-ns constant-NVT (300K) simulation was performed to complete the equilibration steps. The temperature was maintained using the Langevin thermostat with a collision frequency of 1.0 ps^{-1}.

The mechanism of the phosphoryl transfer reaction was studied using the structure obtained after the equilibration steps described above. The interface between the protomers B and C, where the T432$^{rot\text{-}A}$ O_γ – CII-ATP P_γ distance was kept short during the 1-μs trajectory, was used. The QM/MM method was used to study the chemical reaction. The QM region consists of the side chains of T432, E318*, and R385*, triphosphate and part of the ribose group (C5', H5'1, and H5'2) of CII-ATP, and Mg^{2+}. Link atoms are introduced to saturate the valence of the QM boundary atoms. To explore the conformational space efficiently, the density-functional-tight-binding method with third-order correction (DFTB3) (61) was chosen as the QM method. The timestep was decreased to 0.5 fs in the QM/MM simulations, and the system was equilibrated using the QM/MM Hamiltonian for 100 ps prior to the following calculations.

To obtain the initial reaction path starting from the reactant state, we performed a metadynamics (metaD) simulation (62) using the defined QM region. The difference ($q_1 = r_2 - r_1$) between two distances, r_1: T432$^{rot\text{-}A}$ O_γ – CII-ATP P_γ and r_2: CII-ATP P_γ – CII-ATP P_β, was chosen as the reaction coordinate (Fig. 3*A*). Although we were interested in the breaking of the CII-ATP P_γ – CII-ATP $O_{3\beta}$ bond, r_2 was used to avoid the effect of permutations between the three CII-ATP O_β atoms. In the metaD simulation, a Gaussian potential of width = 0.20 Å and height = 0.10 kcal mol^{-1} was added every 0.1 ps. Half-harmonic potentials at $q_1 \geqq 5.7$ Å and $q_1 \leqq 3.3$ Å with a force constant of 100.0 kcal mol^{-1} Å^2. The metaD simulation was performed for 300 ps.

To calculate the free energy profile of the reaction, replica exchange umbrella sampling (REUS) simulations were performed (63). The reaction was divided into two parts: the initial CII-ATP P_γ – CII-ATP $O_{3\beta}$ bond dissociation, which leads to an intermediate state, and the subsequent T432$^{rot\text{-}A}$ O_γ – CII-ATP P_γ bond formation coupled with the proton transfer from T432$^{rot\text{-}A}$ O_γ to E318* O_ε. In the first part, one-dimensional (1D) REUS was performed using q_1, whereas in the second part, we performed two-dimensional (2D) REUS using two collective variables (Fig. 3*A*): q_1 and the proton transfer variable $q_2 = r_4 - r_3$, defined as the difference between two distances, r_3: E318* O_ε – T432$^{rot\text{-}A}$ H_γ and r_4: T432$^{rot\text{-}A}$ O_γ – T432$^{rot\text{-}A}$ H_γ. Harmonic restraints were applied along each coordinate with a force constant of 100.0 kcal mol^{-1} Å^{-2} in 1D-REUS, and 50.0 kcal mol^{-1} Å^{-2} and 25.0 kcal mol^{-1} Å^{-2} along q_1 and q_2, respectively, in 2D-REUS. The restraints were centered at $q_1 = -1.0, -0.8, \ldots 2$ in 1D-REUS, and $q_1 = 1.6, 1.8, \ldots 3.4$ and $q_2 = -1.5, -1.0, \ldots 2.0$ in 2D-REUS. The number of replicas in the 1D- and 2D-REUS simulations were thus 16 and 80, respectively.

The rate of exchange attempts between replicas was fixed at 1 ps in all REUS calculations. The initial structures of the replicas were taken from the snapshots along the metaD trajectory. In the 2D-REUS simulations, the initial structures were further generated by consecutively performing short (20 ps) 2D-umbrella sampling simulations from the metaD snapshots along the positive and negative q_2-directions.

The replica was run for 820 and 620 ps in the 1D- and 2D-REUS simulations, respectively. The initial 120 ps was considered as the equilibration step and thus discarded from the following analyses. The 1D and 2D free energy surfaces (Fig. 3*C* and 3*D*) were constructed by the weighted histogram analysis method (64). The 1D free energy profile for the second part of the reaction was obtained as the minimum free energy path in the 2D free energy surface of q_1 and q_2.

To complement the QM/MM simulations and to explore the conformational states, e.g., the T432 rotamers in solution, MD simulation using classical mechanical force fields was performed from the equilibrated structure described above. The time step was set to 2 fs, and the MD simulation was performed under the constant-NVT (300K) condition for 1 μs.

Acknowledgments

The calculations are partially carried out at the Research Center for Computational Sciences in Okazaki (23-IMS-C111 to T.M. and 23-IMS-C196 to S.S.). This study was supported by Grants-in-Aid for Scientific Research (22H04984, 22K19279, and 23H02448 to S.A.; 22K15051 to Y.F.; 22H02035 and 23K23303 to T.M; and 21H04676 and 23K17361 to S.S.), and partly by Takeda Science Foundation (to S.A.) and Toyoaki Scholarship Foundation (to S.A.).

References

1. C. S. Pittendrigh, Temporal organization: reflections of a Darwinian clock-watcher. *Annu. Rev. Physiol.* **55**, 16-54 (1993).
2. D. Bell-Pedersen *et al.*, Circadian rhythms from multiple oscillators: lessons from diverse organisms. *Nat. Rev. Genet.* **6**, 544-556 (2005).
3. J. S. Takahashi, H. K. Hong, C. H. Ko, E. L. McDearmon, The genetics of mammalian circadian order and disorder: implications for physiology and disease. *Nat. Rev. Genet.* **9**, 764-775 (2008).
4. C. L. Partch, Orchestration of Circadian Timing by Macromolecular Protein Assemblies. *J. Mol. Biol.* **432**, 3426-3448 (2020).
5. R. Narasimamurthy, D. M. Virshup, The phosphorylation switch that regulates ticking of the circadian clock. *Mol. Cell* **81**, 1133-1146 (2021).
6. J. Tomita, M. Nakajima, T. Kondo, H. Iwasaki, No transcription-translation feedback in circadian rhythm of KaiC phosphorylation. *Science* **307**, 251-254 (2005).
7. J. C. Dunlap *et al.*, Chronobiology: Biological Timekeeping (Book). *Choice: Current Reviews for Academic Libraries* **41**, 934 (2004).
8. M. Nakajima *et al.*, Reconstitution of circadian oscillation of cyanobacterial KaiC phosphorylation in vitro. *Science* **308**, 414-415 (2005).
9. A. G. Chavan *et al.*, Reconstitution of an intact clock reveals mechanisms of circadian timekeeping. *Science* **374**, eabd4453 (2021).
10. R. Reinhardt, T. A. Leonard, A critical evaluation of protein kinase regulation by activation loop autophosphorylation. *eLife* **12** (2023).
11. M. Ishiura *et al.*, Expression of a gene cluster kaiABC as a circadian feedback process in cyanobacteria. *Science* **281**, 1519-1523 (1998).
12. R. Pattanayek *et al.*, Visualizing a circadian clock protein: crystal structure of KaiC and functional insights. *Mol. Cell* **15**, 375-388 (2004).
13. T. Nishiwaki *et al.*, Role of KaiC phosphorylation in the circadian clock system of *Synechococcus elongatus* PCC 7942. *Proc. Natl. Acad. Sci. U. S. A.* **101**, 13927-13932 (2004).
14. T. Nishiwaki *et al.*, A sequential program of dual phosphorylation of KaiC as a basis for circadian rhythm in cyanobacteria. *EMBO J.* **26**, 4029-4037 (2007).

15. M. J. Rust, J. S. Markson, W. S. Lane, D. S. Fisher, E. K. O'Shea, Ordered phosphorylation governs oscillation of a three-protein circadian clock. *Science* **318**, 809-812 (2007).
16. I. Vakonakis *et al.*, NMR structure of the KaiC-interacting C-terminal domain of KaiA, a circadian clock protein: implications for KaiA-KaiC interaction. *Proc. Natl. Acad. Sci. U. S. A.* **101**, 1479-1484 (2004).
17. R. Pattanayek *et al.*, Analysis of KaiA-KaiC protein interactions in the cyano-bacterial circadian clock using hybrid structural methods. *EMBO J.* **25**, 2017-2028 (2006).
18. T. Mori *et al.*, Revealing circadian mechanisms of integration and resilience by visualizing clock proteins working in real time. *Nat. Commun.* **9**, 3245 (2018).
19. Y. Murayama *et al.*, Tracking and visualizing the circadian ticking of the cyanobacterial clock protein KaiC in solution. *EMBO J.* **30**, 68-78 (2011).
20. A. Mukaiyama *et al.*, Conformational rearrangements of the C1 ring in KaiC measure the timing of assembly with KaiB. *Sci. Rep.* **8**, 8803 (2018).
21. A. Mukaiyama, Y. Furuike, E. Yamashita, S. Akiyama, Highly sensitive tryptophan fluorescence probe for detecting rhythmic conformational changes of KaiC in the cyanobacterial circadian clock system. *Biochem. J.* **479**, 1505-1515 (2022).
22. Y. Furuike *et al.*, Elucidation of master allostery essential for circadian clock oscillation in cyanobacteria. *Sci. Adv.* **8**, eabm8990 (2022).
23. T. Mori, S. Saito, Conformational Excitation and Nonequilibrium Transition Facilitate Enzymatic Reactions: Application to Pin1 Peptidyl-Prolyl Isomerase. *J. Phys. Chem. Lett.* **10**, 474-480 (2019).
24. R. Pattanayek *et al.*, Structures of KaiC Circadian Clock Mutant Proteins: A New Phosphorylation Site at T426 and Mechanisms of Kinase, ATPase and Phosphatase. *PLoS One* **4** (2009).
25. Y. Furuike *et al.*, Regulation mechanisms of the dual ATPase in KaiC. *Proc. Natl. Acad. Sci. U. S. A.* **119**, e2119627119 (2022).
26. Y. G. Chang, N. W. Kuo, R. Tseng, A. LiWang, Flexibility of the C-terminal, or CII, ring of KaiC governs the rhythm of the circadian clock of cyanobacteria. *Proc. Natl. Acad. Sci. U. S. A.* **108**, 14431-14436 (2011).
27. Y. Furuike, E. Yamashita, S. Akiyama, Structure-function relationship of KaiC around dawn. *Biophys. and Physicobiol.* **21** (2024).
28. J. K. Lassila, J. G. Zalatan, D. Herschlag, Biological phosphoryl-transfer reactions: understanding mechanism and catalysis. *Annu. Rev. Biochem.* **80**, 669-702 (2011).
29. D. Roston, X. Lu, D. Fang, D. Demapan, Q. Cui, Analysis of Phosphoryl-Transfer Enzymes with QM/MM Free Energy Simulations. *Methods Enzymol.* **607**, 53-90 (2018).
30. Y. H. Cheng, Y. K. Zhang, J. A. McCammon, How does the cAMP-dependent protein kinase catalyze the phosphorylation reaction: An ab initio QM/MM study. *J. Am. Chem. Soc.* **127**, 1553-1562 (2005).
31. M. Valiev, J. Yang, J. A. Adams, S. S. Taylor, J. H. Weare, Phosphorylation reaction in cAPK protein kinase-free energy quantum mechanical/molecular mechanics simulations. *J. Phys. Chem. B* **111**, 13455-13464 (2007).
32. A. Perez-Gallegos, M. Garcia-Viloca, A. Gonzalez-Lafont, J. M. Lluch, A QM/MM study of the associative mechanism for the phosphorylation reaction catalyzed by protein kinase A and its D166A mutant. *J. Comput. Aided. Mol. Des.* **28**, 1077-1091 (2014).
33. A. Pérez-Gallegos, M. Garcia-Viloca, À. González-Lafont, J. M. Lluch, SP20 Phosphorylation Reaction Catalyzed by Protein Kinase A: QM/MM Calculations Based on Recently Determined Crystallographic Structures. *ACS Catal.* **5**, 4897-4912 (2015).
34. A. Perez-Gallegos, M. Garcia-Viloca, A. Gonzalez-Lafont, J. M. Lluch, A QM/MM study of Kemptide phosphorylation catalyzed by protein kinase A. The role of Asp166 as a general acid/base catalyst. *Phys. Chem. Chem. Phys.* **17**, 3497-3511 (2015).
35. M. De Vivo, A. Cavalli, P. Carloni, M. Recanatini, Computational study of the phosphoryl transfer catalyzed by a cyclin-dependent kinase. *Chemistry* **13**, 8437-8444 (2007).

36. R. Recabarren, E. H. Osorio, J. Caballero, I. Tunon, J. H. Alzate-Morales, Mechanistic insights into the phosphoryl transfer reaction in cyclin-dependent kinase 2: A QM/MM study. *PLoS One* **14**, e0215793 (2019).
37. G. K. Smith, Z. Ke, H. Guo, A. C. Hengge, Insights into the phosphoryl transfer mechanism of cyclin-dependent protein kinases from ab initio QM/MM free-energy studies. *J. Phys. Chem. B* **115**, 13713-13722 (2011).
38. J. McClory, G. X. Hu, J. W. Zou, D. J. Timson, M. Huang, Phosphorylation Mechanism of N-Acetyl-l-glutamate Kinase, a QM/MM Study. *J. Phys. Chem. B* **123**, 2844-2852 (2019).
39. M. Sanchez-Martinez, E. Marcos, R. Tauler, M. Field, R. Crehuet, Conformational compression and barrier height heterogeneity in the N-acetylglutamate kinase. *J. Phys. Chem. B* **117**, 14261-14272 (2013).
40. S. R. Hubbard, L. Wei, L. Ellis, W. A. Hendrickson, Crystal structure of the tyrosine kinase domain of the human insulin receptor. *Nature* **372**, 746-754 (1994).
41. F. Sicheri, I. Moarefi, J. Kuriyan, Crystal structure of the Src family tyrosine kinase Hck. *Nature* **385**, 602-609 (1997).
42. W. Xu, S. C. Harrison, M. J. Eck, Three-dimensional structure of the tyrosine kinase c-Src. *Nature* **385**, 595-602 (1997).
43. F. von Raussendorf, A. de Ruiter, T. A. Leonard, A switch in nucleotide affinity governs activation of the Src and Tec family kinases. *Sci. Rep.* **7**, 17405 (2017).
44. Q. Wang *et al.*, Autoinhibition of Bruton's tyrosine kinase (Btk) and activation by soluble inositol hexakisphosphate. *eLife* **4** (2015).
45. J. Goldberg, A. C. Nairn, J. Kuriyan, Structural basis for the autoinhibition of calcium/calmodulin-dependent protein kinase I. *Cell* **84**, 875-887 (1996).
46. P. Rellos *et al.*, Structure of the CaMKIIdelta/calmodulin complex reveals the molecular mechanism of CaMKII kinase activation. *PLoS Biol.* **8**, e1000426 (2010).
47. O. S. Rosenberg, S. Deindl, R. J. Sung, A. C. Nairn, J. Kuriyan, Structure of the autoinhibited kinase domain of CaMKII and SAXS analysis of the holoenzyme. *Cell* **123**, 849-860 (2005).
48. C. Kim, C. Y. Cheng, S. A. Saldanha, S. S. Taylor, PKA-I holoenzyme structure reveals a mechanism for cAMP-dependent activation. *Cell* **130**, 1032-1043 (2007).
49. J. Gebel *et al.*, p63 uses a switch-like mechanism to set the threshold for induction of apoptosis. *Nat. Chem. Biol.* **16**, 1078-1086 (2020).
50. J. A. Adams, M. L. Mcglone, R. Gibson, S. S. Taylor, Phosphorylation Modulates Catalytic Function and Regulation in the Camp-Dependent Protein-Kinase. *Biochemistry* **34**, 2447-2454 (1995).
51. J. W. Orr, A. C. Newton, Requirement for Negative Charge on Activation Loop of Protein-Kinase-C. *J. Biol. Chem.* **269**, 27715-27718 (1994).
52. A. J. Ablooglu, R. A. Kohanski, Activation of the insulin receptor's kinase domain changes the rate-determining step of substrate phosphorylation. *Biochemistry* **40**, 504-513 (2001).
53. R. J. Boerner *et al.*, Correlation of the phosphorylation states of pp60c-src with tyrosine kinase activity: the intramolecular pY530-SH2 complex retains significant activity if Y419 is phosphorylated. *Biochemistry* **35**, 9519-9525 (1996).
54. Y. Furuike, J. Abe, A. Mukaiyama, S. Akiyama, Accelerating in vitro studies on circadian clock systems using an automated sampling device. *Biophys. Physicobiol.* **13**, 235-241 (2016).
55. K. Lindorff-Larsen *et al.*, Improved side-chain torsion potentials for the Amber ff99SB protein force field. *Proteins-Structure Function and Bioinformatics* **78**, 1950-1958 (2010).
56. K. L. Meagher, L. T. Redman, H. A. Carlson, Development of polyphosphate parameters for use with the AMBER force field. *J. Comput. Chem.* **24**, 1016-1025 (2003).
57. W. L. Jorgensen, J. Chandrasekhar, J. D. Madura, R. W. Impey, M. L. Klein, Comparison of Simple Potential Functions for Simulating Liquid Water. *J. Chem. Phys.* **79**, 926-935 (1983).
58. T. Darden, D. York, L. Pedersen, Particle Mesh Ewald - an N.Log(N) Method for Ewald Sums in Large Systems. *J. Chem. Phys.* **98**, 10089-10092 (1993).

59. D. A. Case *et al*., AMBER18 (University of California, San Francisco, 2018).
60. M. Bonomi *et al.*, PLUMED: A portable plugin for free-energy calculations with molecular dynamics. *Comput. Phys. Commun.* **180**, 1961-1972 (2009).
61. M. Gaus, Q. A. Cui, M. Elstner, DFTB3: Extension of the Self-Consistent-Charge Density-Functional Tight-Binding Method (SCC-DFTB). *J. Chem. Theory Comput.* **7**, 931-948 (2011).
62. A. Laio, M. Parrinello, Escaping free-energy minima. *Proc. Natl. Acad. Sci. U. S. A.* **99**, 12562-12566 (2002).
63. Y. Sugita, A. Kitao, Y. Okamoto, Multidimensional replica-exchange method for free-energy calculations. *J. Chem. Phys.* **113**, 6042-6051 (2000).
64. S. Kumar, D. Bouzida, R. H. Swendsen, P. A. Kollman, J. M. Rosenberg, The Weighted Histogram Analysis Method for Free-Energy Calculations on Biomolecules .1. The Method. *J. Comput. Chem.* **13**, 1011-1021 (1992).

Figures and Tables

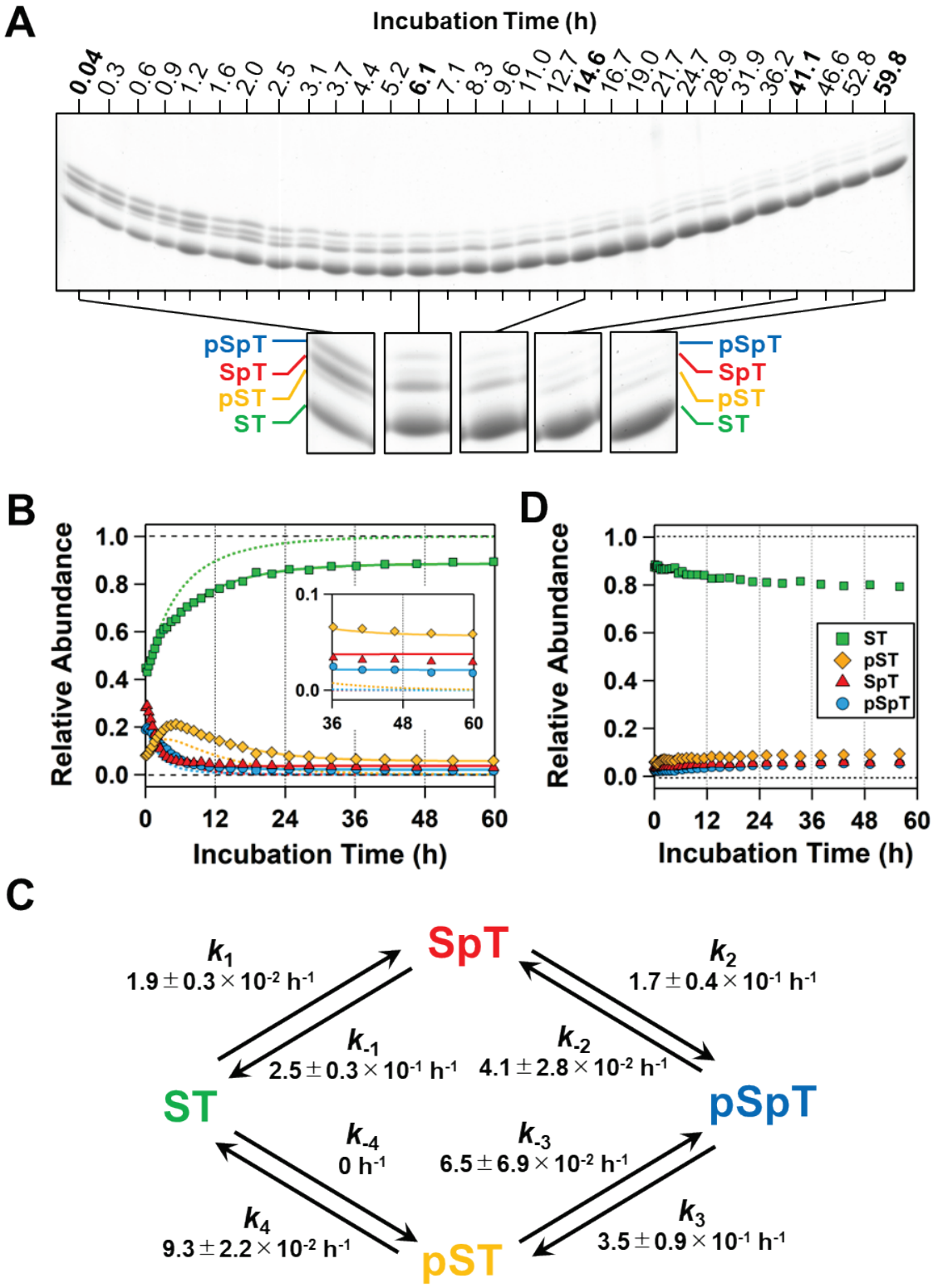

Figure 1. Priming phosphorylation of T432 in KaiC in the absence of KaiA**.** (*A*) Representative image of an SDS-PAGE gel loaded with samples from KaiC under autodephosphorylation conditions at 30°C. To improve the visualization of the four bands corresponding to ST, SpT, pSpT, and SpT, the lanes containing the samples collected at 0.04, 6.1, 14.6, 41.1, and 59.8 h are shown in enlarged images. The whole image of the SDS-PAGE gel is available in *SI Appendix*, Fig. S1. (*B*) Densitometric analysis of the gel image in panel *A* was performed to determine the time course of the relative abundance of the ST (green squares), SpT (red triangles), pSpT (blue circles), and SpT (orange diamonds) forms. The solid lines represent the best fit from global nonlinear least-squares analysis using the four-state model in panel *C*. The inset shows the enlarged plots corresponding to the longer period region. Converged rate constants are compiled in *SI Appendix*, Table S1. The dashed lines represent the worse fit obtained by forcing the rate constants for priming (k_1: ST → SpT) and secondary (k_2: SpT → pSpT) phosphorylation to zero and leaving the others unchanged. (*C*) Reversible four-state cyclic model for KaiC phosphorylation/dephosphorylation. Each step (x = 1, 2, 3, and 4) consists of forward (k_X) and backward (k_{-X}) reactions. (*D*) Autophosphorylation of KaiC was induced at 30°C in the absence of KaiA by increasing the pH from 8.0 to 9.0. The original data for this plot are shown in *SI Appendix*, Fig. S3.

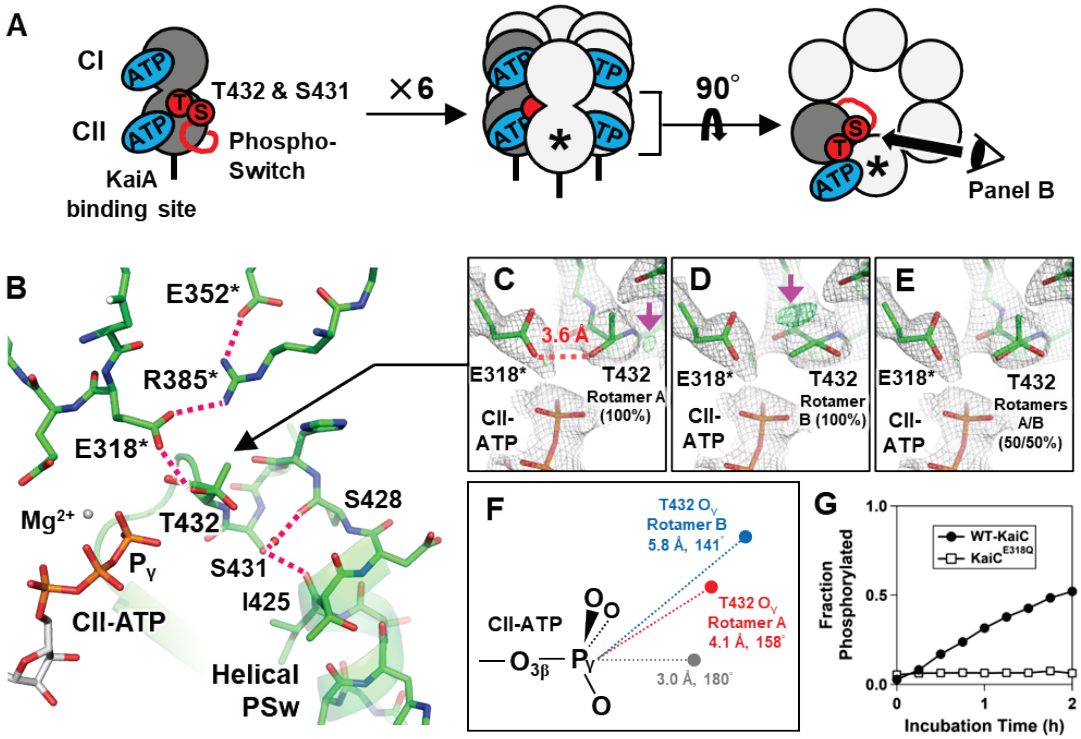

Figure 2. Structure of KaiC-ST. (*A*) Overall structure of the KaiC-ST hexamer. (*B*) Enlarged image of the autokinase active site around CII-ATP. Hydrogen bonds between the phosphorylation sites (S431 and T432), E318*, R385*, E352*, and PSw are indicated by magenta dashed lines. Residues from a neighboring protomer are indicated by asterisks. (*C*–*E*) Occupancy of two rotamers of the T432 side chain. The 2|Fo|–|Fc| (gray mesh) and |Fo|–|Fc| difference maps (green mesh) are countered at 1.0- and 3.0-sigma levels, respectively. Magenta arrows indicate the emerged peaks in the |Fo|–|Fc| difference maps. (*F*) Schematic drawing of the positions of T432 O_γ in rotamers A and B. (*G*) Time courses of phosphorylated fraction for wild-type KaiC and KaiC^{E318Q} after KaiA addition (0.04 mg/mL) at time zero.

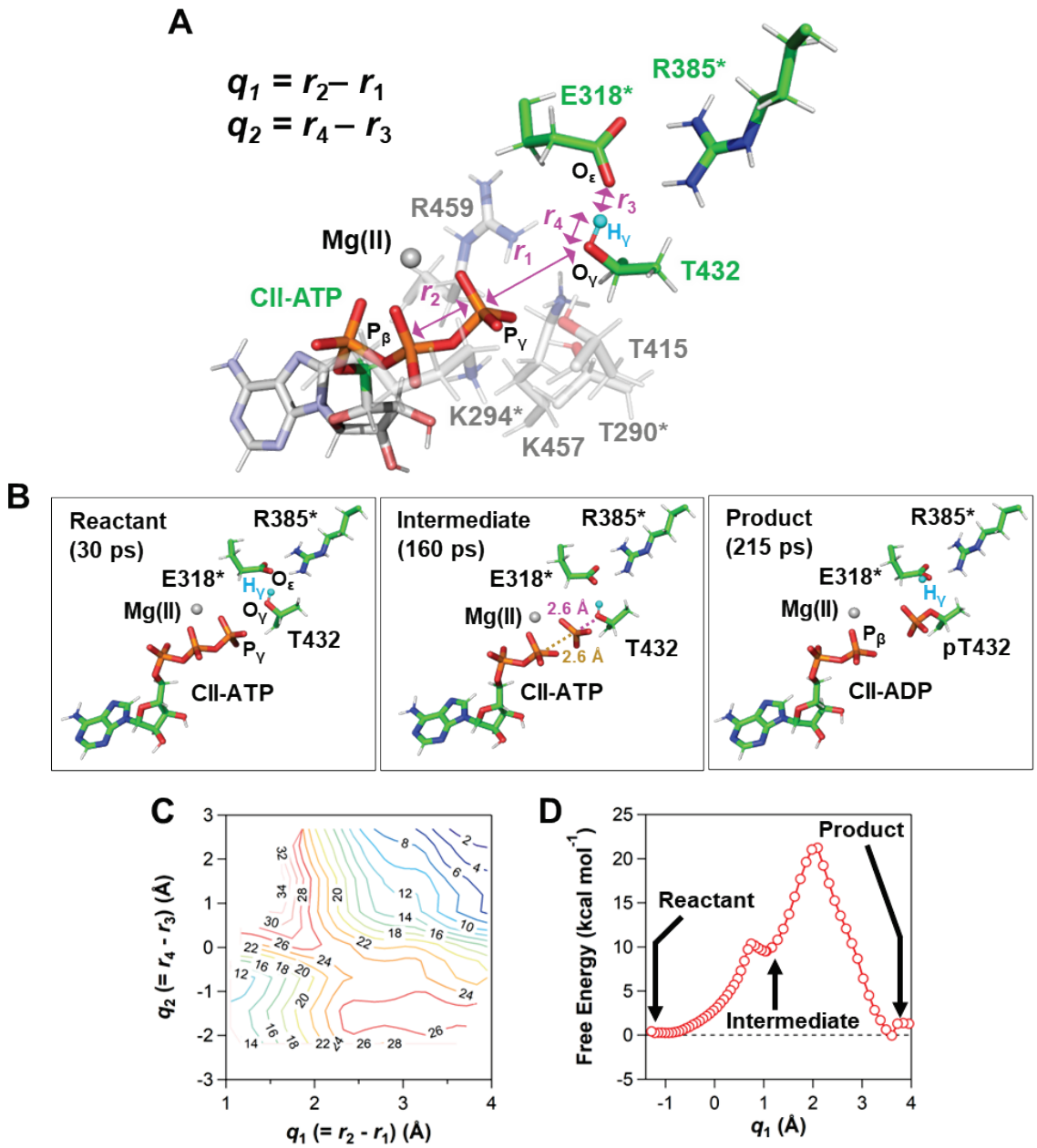

Figure 3. QM/MM simulations of the phosphoryl transfer from CII-ATP to T432. (*A*) Definition of the QM region and reaction coordinates. The QM region consists of the side chains of T432, E318*, and R385*, triphosphate and part of the ribose group (C5', H5'1, and H5'2) of CII-ATP, and Mg^{2+} (green or orange stick models). The hydrogen atom (T432 H_γ) which is transferred from T432 to E318* is highlighted (a cyan sphere). Reaction coordinates are defined as $q_1 = r_2 - r_1$ (r_1: CII-ATP P_γ – T432 O_γ, r_2: CII-ATP P_γ – CII-ATP P_β) and $q_2 = r_4 - r_3$ (r_3: T432 H_γ – E318* O_ε, r_4: T432 H_γ – T432 O_γ). (*B*) Structures obtained during the QM/MM metaD simulation of T432 phosphorylation in KaiC-ST. (*C*) Two-dimensional free energy surface calculated using the QM region defined in panel *A*. (*D*) Free energy surface along q_1 from the QM/MM calculation.

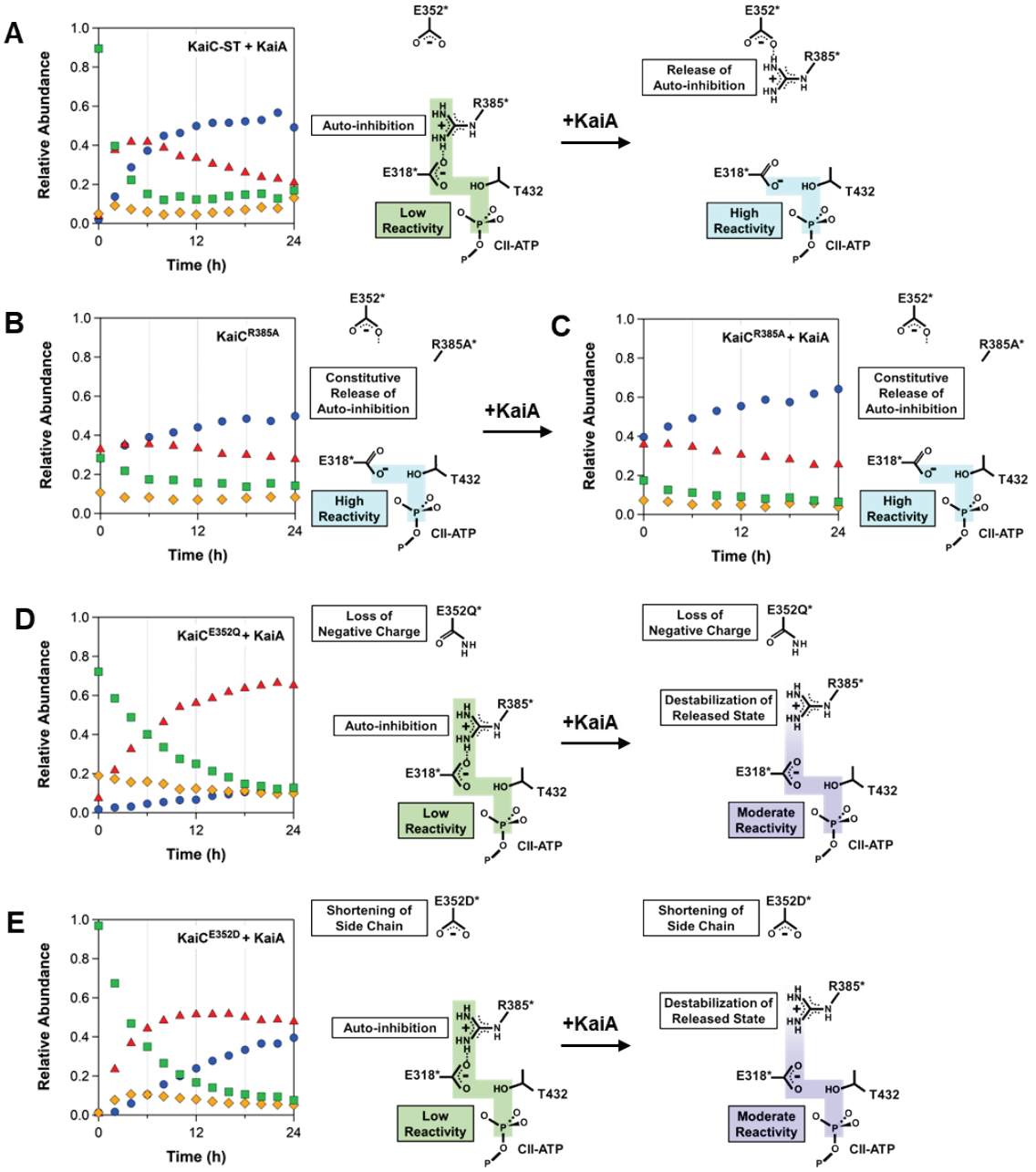

Figure 4. Indirect effects of the E318*-mediated regulation of the nucleophilicity of T432$^{rot\text{-}A}$ O_γ. (*A*–*E*) Time courses of four phosphorylation states (ST: green squares, SpT: red triangles, pST: orange diamonds, and pSpT: blue circles) for KaiC-ST (+KaiA), KaiC^{R385A} (–KaiA), KaiC^{R385A} (+KaiA), KaiC^{E352Q} (+KaiA), and KaiC^{E352D} (+KaiA), respectively, at 30°C. The schematic drawing shown in each panel illustrates possible hydrogen bonds (black dotted line) and T432$^{rot\text{-}A}$ H_γ-withdrawing reactivity of E318* (green, cyan and purple backgrounds) to enhance the nucleophilicity of T432$^{rot\text{-}A}$ O_γ. KaiC-ST, KaiC^{E352Q}, and KaiC^{E352D} (0.2 mg/mL) were pre-incubated at 30°C for 48 h and then at time zero mixed with KaiA at a final concentration of 0.04 mg/mL. KaiC^{R385A} (0.2 mg/mL), which was purified and stored in a freezer before use, was directly incubated at 30°C with or without KaiA (0.04 mg/mL).

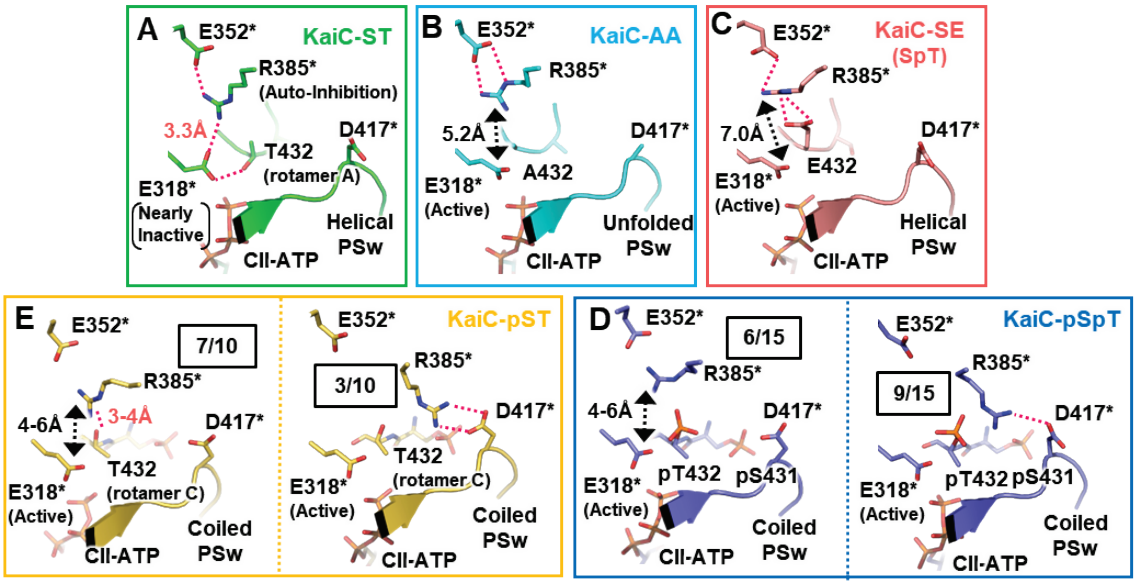

Figure 5. R385* rearrangement during the circadian cycle. The side chain orientations of R385* in (*A*) KaiC-ST (PDB code: 7DYJ), (*B*) KaiC-AA (PDB code: 7DYE), (*C*) KaiC-SpT (PDB code: 7DYI), (*D*) KaiC-pSpT (PDB code: 7DXQ, 7DY1, and 7V3X), and (*E*) KaiC-pST (PDB code: 7DY1, 7V3X, and 7DY2) are shown. The numbers enclosed in boxes indicate the fractions of the protomers with the corresponding conformation of R385* in the structure library. Hydrogen bonds are indicated by magenta dashed lines. Inter-atomic distances beyond hydrogen bonding distance are indicated by black dashed arrows.

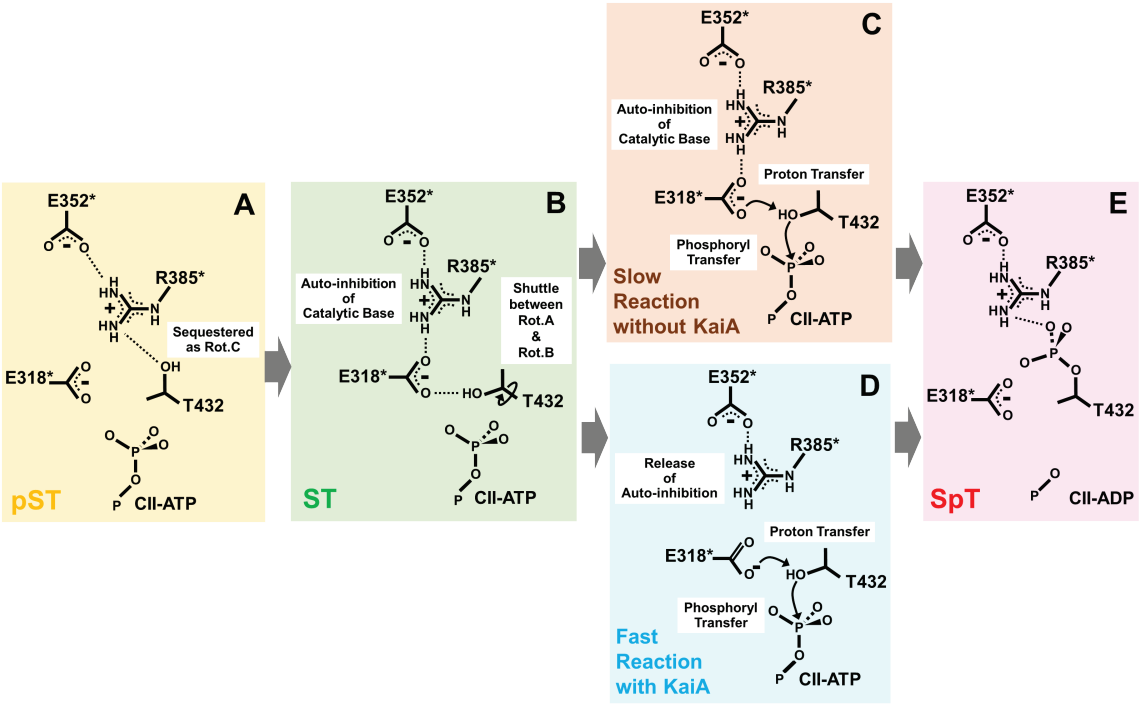

Figure 6. Proposed reaction scheme for priming phosphorylation at T432 in KaiC. (*A*) KaiC-pST, (*B*) KaiC-ST, (*C*) A reaction intermediate without KaiA, (*D*) the KaiA-assisted state, and (*E*) KaiC-SpT, respectively.